Characterization and Performance of TiO_2 Nanoparticles Prepared by Microwave in Different Mixtures of Water and Ethylene Glycol for the Food Dye E131 VF Degradation

F. Kassir[1], M-A. Azoury[1], P. Damacet[1], Z. Harajli[3], M. El Jamal[1*] and A. Ebrahimian Pirbazari[2*]

[1]*Inorganic and Organometallic Coordination Chemistry Laboratory (LCIO), Faculty of Sciences (I), Lebanese University, Rafic Hariri Campus, El Hadath, Lebanon*
[2]*Hybrid Nanomaterials & Environment Lab, Fouman Faculty of Engineering, College of Engineering, University of Tehran, Fouman, Iran*
[3]*Physics Department, American University of Beirut, Lebanon*
*Corresponding authors: mjamal@ul.edu.lb and aebrahimian@ut.ac.ir

Received 26/11/2021; accepted 15/03/2022
https://doi.org/10.4152/pea.2023410305

Abstract
In this research, TiO_2 NP were prepared by MW-R and conventional SG methods, using TTIP as Ti precursor, in the presence of different mixtures of distilled H_2O and ETG ($0 < H_2O/ETG < 100\%$), as a solvent. The prepared samples were characterized by XRD, Raman, FTIR, EDX/ SEM, N_2 physisorption, DLS and UV/visible DRS techniques. XRD and Raman analyses showed that Ant phase dominated, with traces of Rt or Brk phases, in some samples. According to K-M curves, TiO_2 calculated E_G decreased with an increase in Rt phase percentage. PC performance of the prepared samples was tested on E131 VF. Kinetic evaluations showed that Rt percentage and surface area had a significant role in TiO_2 NP PC performance. E131 VF degradation high RC were obtained in an AU by 0% ETG SG (0.130 (AU)) and 0% ETG MW-R (0.113 (AU)), due to the high surface area and Rt absence. The samples (x% ETG) synthesized by the MW-R method showed low pore volume and PC performance that might have been be due to a blockage of the pores and screening effect of some combustion products or residual ETG, which carried UV irradiation to the catalyst surface.

***Keywords*:** MW-R, SG, TiO_2, ETG and PC degradation.

Introduction•

In recent years, the quality of water resources has been affected, due to population increase, industrial production, intensive agriculture and rising urbanization. Domestic

• The abbreviations and symbols definition lists are in pages 259 and 260.

and industrial effluents contain various organic and inorganic contaminants that are discharged into the environment and pollute it [1]. To prevent the shortage of clean water in water-stressed nations, the reuse and treatment of municipal and rural effluents, for industrial and agricultural purposes, can be the best solution [2]. Over 7 x 10^5 tons of dyes and pigments are produced every year, and 10 to 15% of them are discharged into the effluents, causing several problems to aquatic life. As worldwide environmental regulations tighten, several methods for removing such dyes have been developed, which are low-cost and high-efficient for treating polluted wastewater [3]. Dyes stability against chemical oxidation methods hinders their removal by traditional biochemical and physicochemical processes [4]. Also, some conventional treatment procedures for wastewater, such as filtration and chemical oxidation, have disadvantages such as their high cost, use of chemical reagents, production of harmful secondary pollutants, and being time-consuming [5]. Due to the above-mentioned reasons, researchers have been looking for more cost-effective purification methods that have high efficiency in the treatment of colored effluents. PC oxidation process, based on semiconductors such as TiO_2, is a low-cost, clean and environmentally friendly method that has attracted the attention of researchers [6, 7]. It has shown high efficiency for the photo-mineralization of a wide range of organic and dyes pollutants, without hazardous byproducts (H_20 and CO_2). The three TiO_2 crystalline polymorphs are Ant, Rt and Brk, which have unique chemical and physical characteristics that make them suitable for various applications. Different methods, such as SG [8, 9], solvothermal [10, 11] and hydrothermal [12] techniques, CVD [13], MWs [14-17] and ultrasounds [18-20], have been reported for TiO_2 NS synthesis, which can control their structural, textural and morphological properties. When the source of organometallic precursors reacts with water, hydrolysis and condensation processes occur simultaneously. Several experimental parameters, such as amounts of raw materials, hydrolysis temperature, stirring conditions and type of organic solvent, affect these two processes [21]. MW-based synthesis method is one of the most low-cost, simple, energy-saving and time-efficient approaches for of TiO_2 NS preparation, which results in better yields with a shorter reaction time [22, 23]. The electromagnetic spectrum MW region is located between infrared and radio waves. The materials interaction with the electromagnetic radiation electric field causes the movement of ions and molecular dipoles, which explains liquids heating by MW. Molecules with μ attempt to align with the produced field, causing rotation and movement. This movement generates kinetic energy that is then transformed into thermal energy and, hence, heat. MW-assisted synthesis has been effectively used for developing a wide variety of inorganic and organic molecules, complexes and NP, as well as industrial processes [23]. Liquids with high molecular dipoles, such as H_2O and ETG, have shown an increase in temperature caused by MW irradiation [24]. H_2O is known to absorb a large amount of MW radiation, due to its polar properties. MW effect on H_2O occurs through its dielectric interaction (dipole induced) with the electric field, which produces thermal energy. ETG is also largely used, due to its high reducing power, BP and δ (197 ºC and 1.350 against 100 ºC and 0.123 for water, respectively) [23].

Most published articles studied the effect of preparation parameters, such as MW power [15], irradiation time [25, 26] and use of a pure solvent, on TiO_2 morphology and phase [16]. In the present study, so as to investigate TiO_2 physicochemical properties and PC efficiency, SG and MW-assisted approaches were used for its NS synthesis. ETG and distilled H_2O were used as solvents, in different proportions, for studying their effect on the morphology of NP synthesized by SG and MW-assisted approaches. PC activity and the transformation of electromagnetic energy into heat are the functions of solvents ratio. The obtained samples were characterized by XRD, EDX/SEM, Raman, FTIR, DLS, N_2 physisorption and UV/visible DRS techniques. PC activity of the NP was studied by E131 VF degradation.

Experimental section

Materials and synthesis details

TTIP (98%) and pure ETG were purchased from Acros Organics. E131 VF, which was selected as an organic pollutant model, was purchased from Sigma Aldrich ($C_{27}H_{31}N_2O_6S_2$-Na; purity: 50%; molecular weight: 565.67 g). Fig. 1 shows the dye structure. The MW reactor used for TiO_2 synthesis was WBFY-201 Microwave Chemical Reactor, designed by Zhengzhou Keda Machinery and Instrument Equipment Co., Ltd.

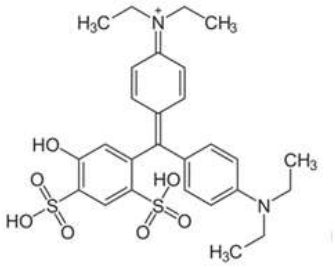

Figure 1. E131 VF structure.

TiO_2 preparation via MW-R method

TiO_2 NP were prepared by a modified assisted MW-irradiation synthesis method [16]. A fixed volume of TTIP (10 mL) and various ratios of distilled H_2O/ETG, as a solvent mixture ($0 < H_2O/ETG < 100\%$), were used. TTIP was added to the solvent mixture and stirred for 40 min. Milky-turbid solutions were obtained with an increasing number of particulates, at higher ETG percentages. The mixture was then put for 10 min in a domestic MW reactor (400 W (2.45 GHz)), for inducing TiO_2 formation, and a reflux apparatus was used during irradiation. The sample was separated, washed several times with H_2O and ethanol, and the pale-yellow precipitate was collected. After drying the samples at 200 ºC, for 2 h, their color changed from yellow to orange. Then, the samples were calcined, at 500 ºC, for 4 h, in air, and their color changed to gray. The prepared TiO_2 samples were named x% ETG MW-R. Some difficulties, such as overheating, prevented the authors of the present study from preparing 100 % ETG MW-R.

TiO_2 preparation via SG method

TiO_2 NP were synthesized by the SG method reported in [27], with some modifications. A mixture of 10 mL TTIP and 100 mL H_2O was stirred for 30 min, at room temperature, and, then, for 4 h, at 65 ºC, so as to form a white gel. The gel was dried at 200 ºC, for 2 h, and a very light-yellow precipitate was obtained. This sample was calcined at 500 ºC, for 4 h, and its color changed to bright white. The sample named 100% H_2O SG was prepared by adding 10 mL TTIP to 100 mL ETG (after calcination, it became light gray).

PC tests

E 131 VF degradation rate was followed by measuring its A at λ_{max} of 640 nm. PC degradation curves were plotted as A (in AU) *vs*. time (in min), for calculating the RC from the nonlinear kinetic model. A suspension containing 0.08 g TiO_2 and a 100 mL E 131 VF aqueous solution (20 mg/L) was stirred in the dark, for 30 min, in order to reach A-D equilibrium. Then, the sample was placed in the photo reactor, irradiated by three UV-C lamps (λ_{max}= 256 nm, 8 W) and placed 10 cm above a glass bowl (Luzchem LZC-4V, Canada), under continuous magnetic stirring. The PC reactor was equipped with a fan, for keeping the temperature at 28 ºC, and eliminating the heat from the lamps. Irradiation tests were done separately by one of three types of lamps: UV-C, UV-A (λ_{max}= 360 nm, 8 W) and visible light lamps (8 W).

Characterization

The machine used for XRD scans was a D8 advance diffractometer, from Bruker AXS systems. The X-ray source consisted of a Cu tube emitting X-rays of K_α radiation, with the λ of 1.5418 Å. Rt phase percentage was obtained by

.

$$Rt\ (weight\ \%) = \frac{1}{(1+0.884\times\frac{I_A}{I_R})} \times 100 \qquad (1)$$

where I_A and I_R are the diffraction intensity of Ant and Rt phases, respectively [27]. TiO_2 mean crystal size was determined by Scherer equation.

$$D = \frac{0.89 \times \lambda}{\beta\ \cos\theta} \qquad (2)$$

where D is the average crystallite size, λ is the x-ray wavelength (0.1541 nm), β represents the FWHM diffraction, in radian, for a peak at 2θ = 25.4°. The samples FTIR spectra, using a KBr pellet, were recorded on a Jasco FT/IR-6300 spectrometer, in the wavenumber range from 400 to 4000 cm^{-1}. Raman spectra were recorded by a Horiba Scientific spectrometer, operated by a green laser, at 532 nm. SEM images were prepared using a MIRA 3 series. Images were taken at several resolution values, in order to obtain a full observation of the surface morphology. An EDX spectrometer detector, attached to SEM, was used to obtain micro-chemical information. UV/visible diffuse reflectance spectra were obtained using a Jasco V-570 spectrophotometer, in order to calculate PC E_G. The prepared samples surface area was determined via a fully automated three-station micromeritics 3Flex surface characterization analyzer, using N_2 gas. TiO_2 particles where degassed and activated at 180 ºC,

overnight, before BET measurements. A NanoPlus Zeta Potential and a NP analyzer were used to perform DLS measurements. The suspension was prepared with 0.1 mg of each sample in 3 mL DMSO.

Results and discussion

XDR analysis

XRD patterns of TiO_2 samples synthesized by MW-assisted approaches are shown in Fig. 2a.

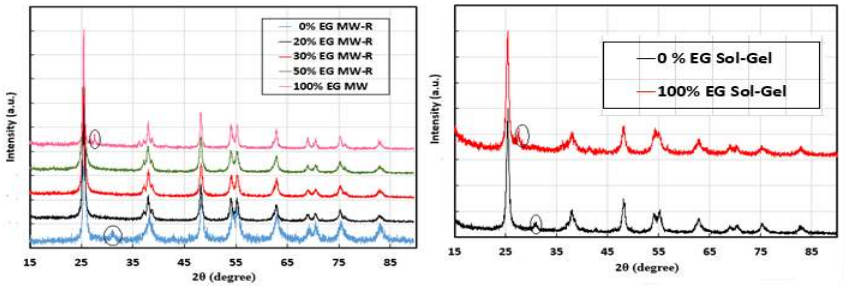

Figure 2. XRD patterns for: **a)** TiO_2 NP prepared by MW-R; **(b)** TiO_2 prepared by SG.

Several major diffractions were observable at 2θ (25.4, 37.8, 48.1, 54, 55.2 and 62.7°), which correspond to the Ant phase reflection [27, 28]. For the 100% ETG MW sample, it occurred a diffraction, at 2θ, of 27.56°, which indicates that Rt phase was also present. In 0% ETG MW-R sample XRD pattern, the diffraction, at 2θ, of 30.8°, was assigned to Brk phase. XRD of the samples prepared by SG technique were not as sharp as those of MW method. The sample prepared with H_2O showed Ant and Brk phases, and the sample prepared by ETG presented Ant and Rt phases (Fig. 2b). Brk phase appearance was probably a critical factor for the inhibition of Ant transformation into Rt, in the samples that were prepared just with pure H_2O.
Rt phase was calculated according to equation 1 (at 2θ of 25.4° (I_A) and 27.3° (I_R)). 9.3 and 20% Rt were obtained for 100% ETG MW and 100% ETG SG samples, respectively (Table 1). The samples prepared by MW-R did not contain Rt phase, except for the sample with 10% ETG (6.3%). Also, TiO_2 crystallites NP average dimensions were estimated by Scherer equation, and are presented in Table 1.

Table 1. Samples average crystal size dimension and Rt phase (%).

Sample	Rt *phase* *%*	*Crystalline size (nm)*
0% ETG MW-R	-	19.5
10% ETG MW-R	6.3%	25.1
20% ETG MW-R	-	21.2
30% ETG MW-R	-	19.2
50% ETG MW-R	-	16.5
100% ETG MW	9.3%	15.1
0% ETG SG	-	15.7
100% ETG SG	20%	15.1

The obtained data show that they decreased with an increase in ETG%. Also, TiO_2 NP samples prepared by SG had a smaller average size than that of the others.

FTIR spectroscopy analysis

The FTIR spectra of the samples prepared by MW-R method, with different ETG percentages, are displayed in Fig. 3a.

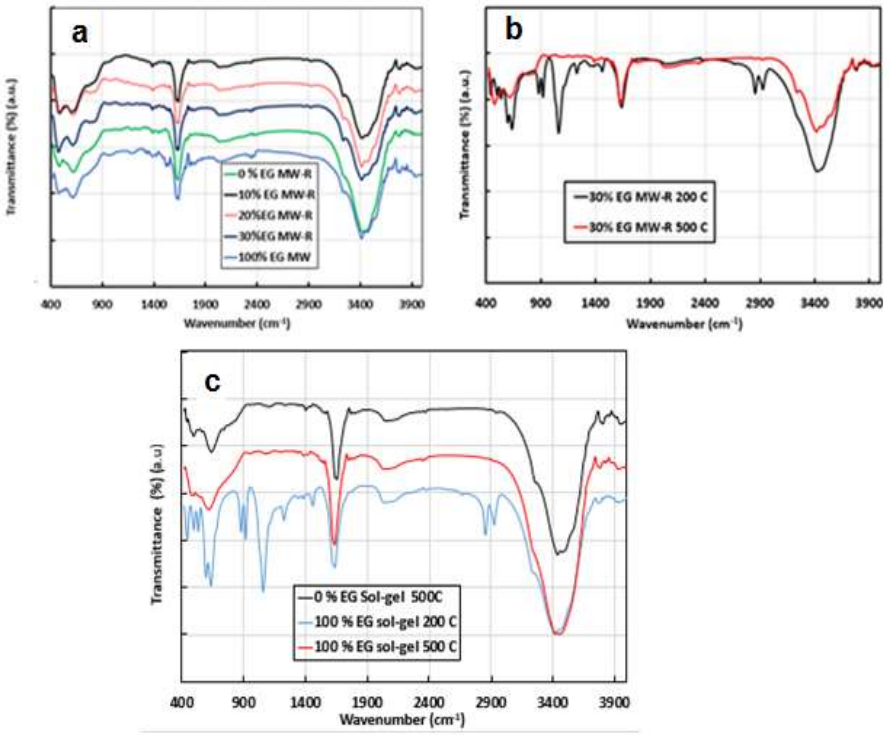

Figure 3. FTIR spectra of TiO_2 samples prepared by: **(a)** MW-R; **(b)** MW-R with 30% ETG at 200 ºC, and calcined at 500 ºC; **(c)** SG method, at 200º C, and calcined at 500 ºC.

The spectra show three distinct vibrations, at 3420, 1620 and 620 cm^{-1}. Vibrations at 3420 and 1620 cm^{-1} are O-H stretching and O-H bending, respectively. They are due to physically adsorbed water molecules from the atmosphere, or to ETG molecules [29]. Hydroxyl groups are necessary for the PC degradation process. They react with photo-induced holes, and produce hydroxyl radicals that are strong oxidants [21]. Vibrations at 476 and 620 cm^{-1} are due to TiO_2 lattice Ti–O and Ti–O–Ti bonds (known as fingerprints) [30]. FTIR spectra of 0 % ETG and 100 % ETG prepared by SG showed similar spectra to those prepared by MW-R (Fig. 3c). The absence of ETG vibrations, which are the alkane C-H stretching at 2900 cm^{-1}, the C-H scissor and bending at 1450-1292 cm^{-1} and the alcohol C-O stretching at 1250 cm^{-1}, confirms the elimination of a large amount of the former, during the samples calcination, or the remaining of it and of some combustion products in the samples pores (not detectable by FTIR) (Figs. 3b and 3c) [31, 32].

Raman spectroscopy analysis

x% ETG MW-R samples Raman spectra consist of six vibrations located at 144, 200, 399, 513, 519 and 639 cm^{-1} (Fig. 4a), which confirm the formation of Ant phase for TiO_2 [33, 34].

The vibrations at 144, 200 and 639 cm^{-1} can be assigned to symmetric stretching vibrations of the O-Ti-O bond (Eg mode). The peak at 513 cm^{-1} (A_{1g} mode) can be attributed to Ant phase O-Ti-O anti-symmetric bending vibration. The magnified Raman spectrum of the 0% ETG MW-R sample (Fig. 4b) shows Brk phase that is characterized by several vibrations in the range from 210 to 330 cm^{-1}, in addition to Ant phase [35].

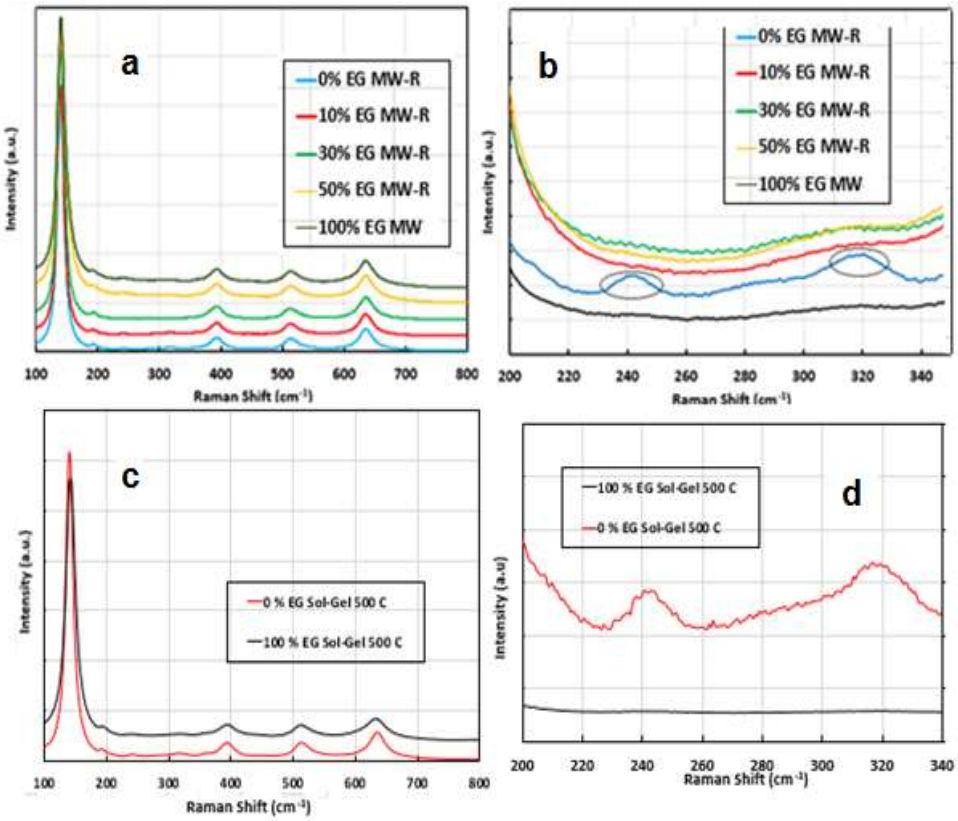

Figure 4. Raman spectra of TiO_2 samples prepared by: **a** and **b -** MW-R; **c** and **d -** SG.

Similar bands were observed with 0 % ETG prepared by SG (Fig. 4d). In the same conditions, the preparation method did not affect TiO_2 phase(s). Rt phase was not detected by Raman technique (nor by XRD) in the samples prepared with ETG. This might be due to the LOD of each technique.

SEM/EDX analysis

SEM images of the TiO_2 prepared samples (Fig. 5) reveal that NP have smooth, irregular shapes and different agglomerate sizes.

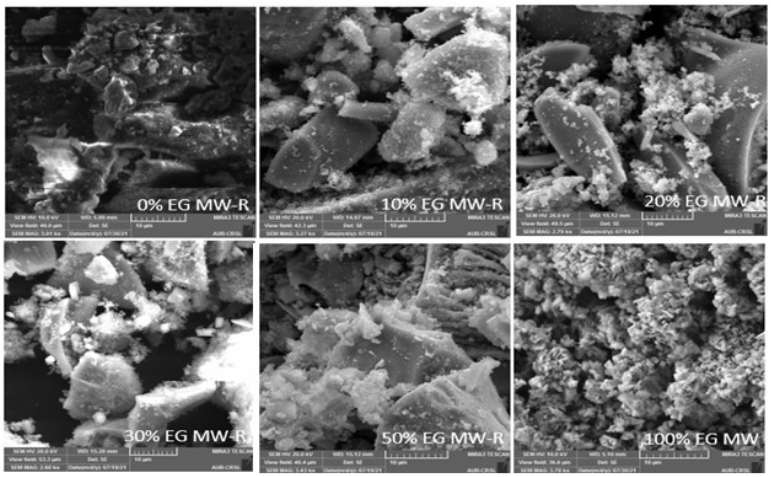

Figure 5. SEM images of TiO_2 samples prepared by MW.

UV/vis DRS analysis

The reflectance spectra were converted to K-M diagrams, using the K-M relation, to calculate the samples E_G (Table 2).

$$[F(R)h\nu]^{0.5} = A(h\nu - E_{bg}) \qquad (3)$$

where A is a constant, F(R) is K-M function, hυ is photon energy and E_{bg} refers to E_G. E_G of the TiO_2 samples prepared with pure distilled H_2O (MW-R or SG) was very close to the Ant reported value (3.10 to 3.20 eV) [27, 36]. TiO_2 Ant and Rt phase E_G were 3.20 and 3.00 eV, respectively.

Table 2. Chemical composition of the prepared samples (Atomic percent: At%)

Sample	C (At %)	O (At %)	Ti (At %)	Ti/O ratio
10% EG MW-R	3.41	71.43	29.23	0.41
20% EG MW-R	1.84	70.06	28.10	0.40
30% EG MW-R	2.85	64.76	32.39	0.50
50% EG MW-R	2.56	66.12	31.32	0.47
100% EG MW	3.09	68.54	35.89	0.52
0% EG Sol-Gel	3.49	70.50	26.10	0.37
100% EG Sol-Gel	3.32	70.79	25.68	0.36

The samples E_G shifted to lower values with higher Rt percentages (Table 3).

Table 3. Samples E_G and Rt phase percentage.

Sample	Rt phase %	E_G (eV)
0% ETG MW-R	-	3.10
10% ETG MW-R	6.3%	2.97
20% ETG MW-R	-	3.10
30% ETG MW-R	-	3.10
50% ETG MW-R	-	3.07
100% ETG MW	9.3%	2.80
0% ETG SG	-	3.20
100% ETG SG	20%	2.94

DLS analysis

DLS particle size distribution shows a skewed Gaussian shape (Fig. 6).

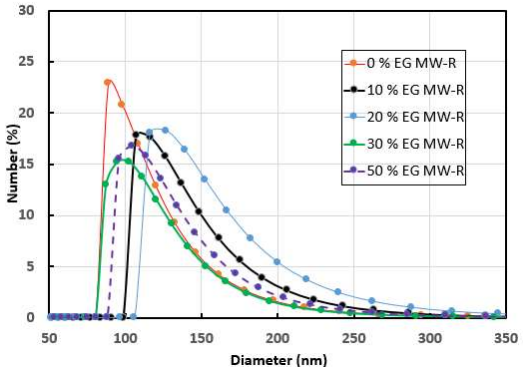

Figure 6. DLS distribution of the samples particle size.

The mean diameter of the samples prepared by the MW-R method is higher than that of P25 (~110 nm) [37]. D50, or mean size of the samples, is high, due to agglomeration [38]. The 0% ETG MW-R sample has the lowest D50 (and mean) and the narrower distribution (PI: 0.64), whereas 20 % ETG MW-R sample has the highest mean and PI (1.5), so there was no correlation between ETG percentage in the mixture (ETG–H_2O) and the samples mean size (Table 4).

Table 4. Characteristic parameters of the samples DLS analysis (PI).

Sample	PI	D10	D50 (*mean*)	D90
0 % ETG MW-R	0.64	84	102 (117)	149
10% ETG MW-R	0.90	103	125 (148)	181
20% ETG MW-R	1.50	111	137 (157)	201
30% ETG MW-R	0.84	86	107 (120)	154
50% ETG MW-R	1.02	93	115 (129)	169
100% ETG MW	3.38	96	118 (131)	162
0% ETG SG	1.78	81	100 (117)	142
100% ETG SG	0.92	100	121 (136)	170

BET analysis

MW-R samples surface area and pore volume significantly decreased with higher ETG percentages (Table 5).

Table 5. Textural properties of the prepared samples.

Sample	Pore volume (cm^3/g)	Average pore diameter (Å)	Pore area (m^2/g)	Surface area (m^2/g)
0% ETG MW R	1.590	165.72	503.1	56.94
10% ETG MW R	0.019	31.53	24.2	14.12
20% ETG MW R	0.021	34.67	24.6	1.78
30% ETG MW R	0.078	36.70	85.6	8.20
50% ETG MW R	0.094	58.20	107.7	5.97
100 % ETG MW	0.156	134.41	203.2	13.27
100% ETG SG	0.304	118.58	115.3	37.07
0% ETG SG	0.948	128.67	389.1	46.74

This may be due to NP aggregations caused be the increase in ETG%. ETG did not disappear totally after two consecutive calcinations, and TiO_2 color was gray. ETG or some products residues during the samples calcination decreased the pores volume and area. The samples synthesized without ETG showed higher surface area and pore volume than those of other samples, regardless of the synthesis method (SG or MW-R) (Table 5). These samples also showed that TTIP is related to mesoporous materials (Fig. 7).

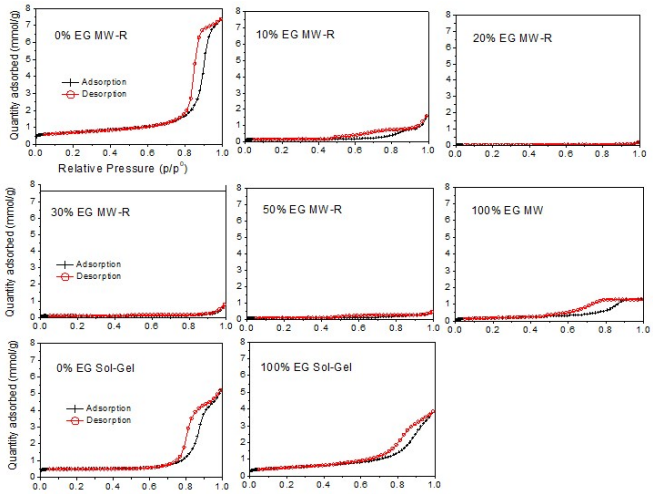

Figure 7. N_2 adsorption-desorption isotherms for the samples.

The samples pores volume distribution is presented in Figs. 8 and 9.

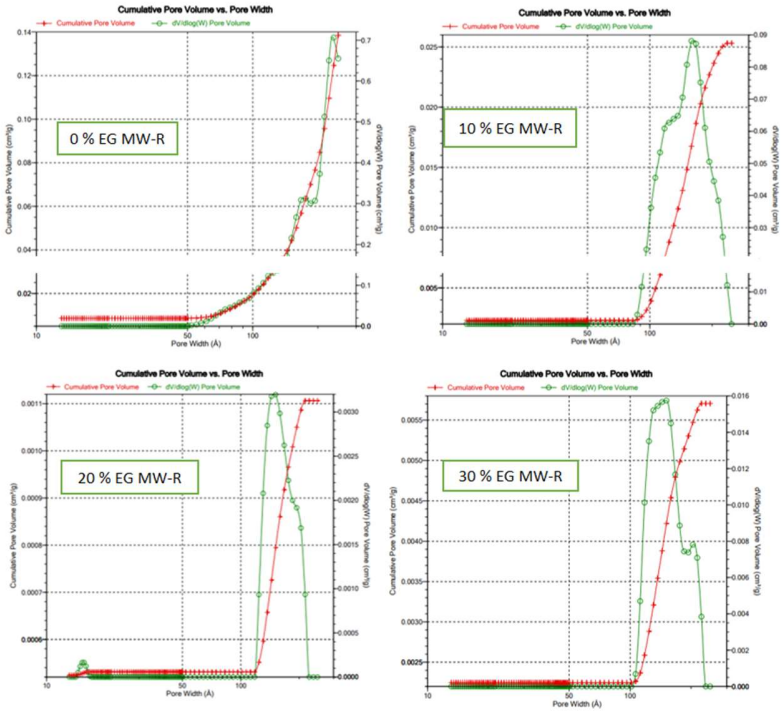

Figure 8. Samples cumulative pore volume *vs* pore width.

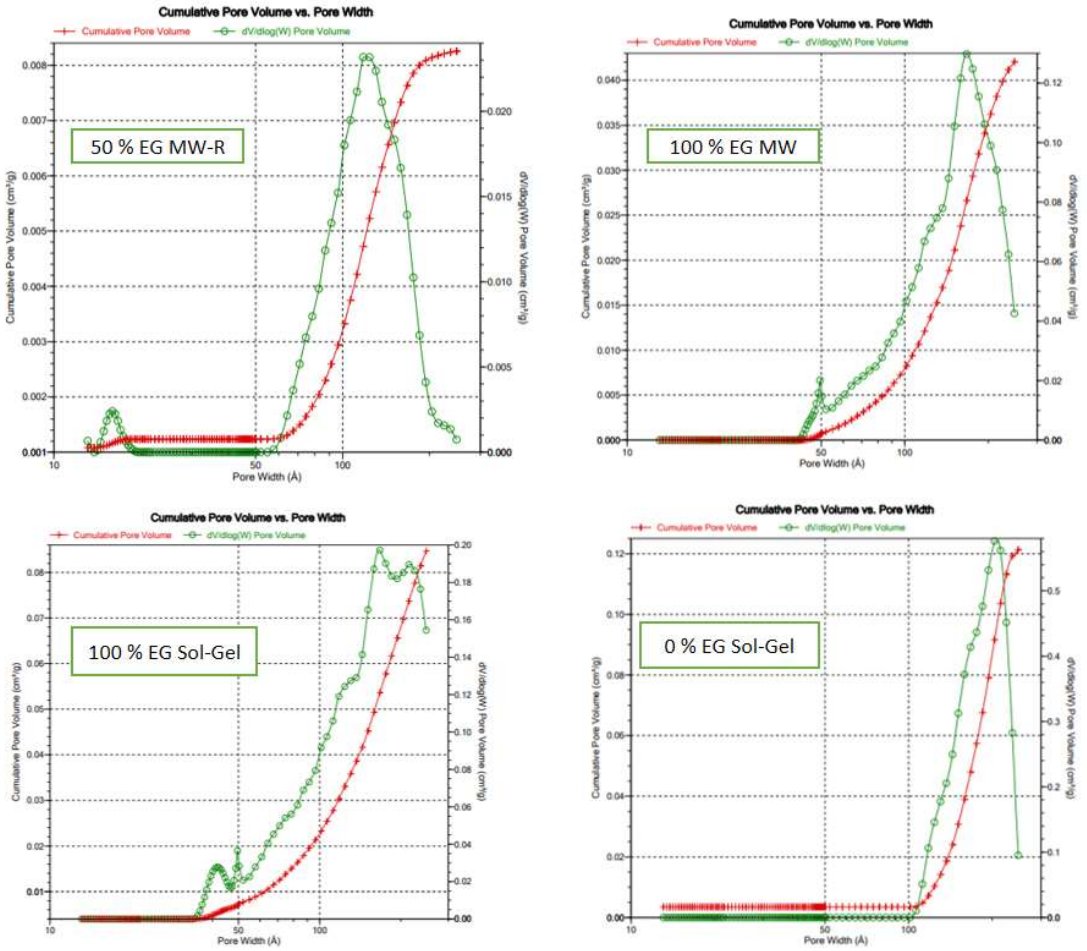

Figure 9. Samples cumulative pore volume *vs* pore width.

E131 VF kinetic photodegradation

The kinetic experiments were performed under different conditions. For the samples photolysis and adsorption tests, the decrease in A value at λ_{max} (640 nm) was less than 10%. Therefore, both photolysis and adsorption phenomena were neglected. In UV-C irradiation and PC presence, 94% dye degradation was obtained, within the same duration. The degradation efficiency was calculated by Equation 4.

$$\text{Degradation Effeciency (\%D)} = \frac{A_0 - A_t}{A_o} \times 100 \quad (4)$$

Fig. 10a displays E131 VF PC degradation in the presence of x% ETG MW-R samples. The dye degradation followed the first-order kinetics that can be represented by: $C = C_o e^{-kt}$ (or $A = A_o\ e^{-kt}$), where C and C_0 are concentration and initial concentration, t is time, A and A_o are absorbance and k is the RC. PC tests were repeated three times, and the average RC obtained by MW-R samples was calculated from the nonlinear kinetic curves in Fig. 10a. Fig. 10c shows RC variation during the photo degradation tests. A decreasing trend in the RC, along with the increase in ETG

percentage, were observed. This it is most probably due to the screening effect of residual ETG (undetectable by FTIR), which prevented the catalyst from absorbing UV radiation, or to ETG or some combustion products that blocked TiO_2 pores. The sample prepared by pure H_2O has shown better PC activity than that of those synthesized by the mixture of ETG and H_2O, due to higher surface area and Rt phase absence. Also, the samples prepared by SG (Fig. 10b) have higher photo activity than those prepared by MW-R (Table 6).

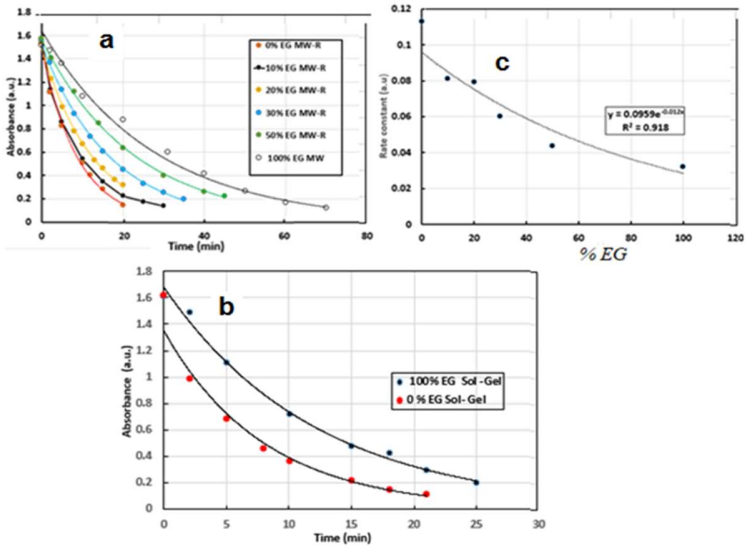

Figure 10. (a) and **(b)**: curves of E131 VF photo degradation by TiO_2 NP; **(c)** RC variation as a function of ETG percentage for MW-R samples.

The difference in the photo activity between the two samples prepared with ETG (gray color of 100 % ETG MW-R and white color of 100 % ETG SG) was due to ETG total elimination in the SG sample, and to a higher surface area. The 0% ETG SG sample showed higher photo activity than that of 100 % ETG SG, because of Rt phase absence, and higher surface area (Table 6). TiO_2 PC activity remained approxim. constant under UV and UV-C, but, under visible light, no degradation occurred.

Table 6. Samples RC, surface area and Rt phase percentage.

Sample	RC (AU)	Surface area (m^2/g)	Rt %
0% ETG MW-R	0.113	56.94	-
10% ETG MW-R	0.081	14.12	6.3%
20% ETG MW-R	0.075	1.78	-
30% ETG-R	0.060	8.20	-
50% ETG MW-R	0.044	5.97	-
100% ETG MW	0.032	13.27	9.3%
100% ETG SG	0.080	37.07	20%
0% ETG SG	0.130	46.74	-

Conclusion

TiO_2 NP were prepared by MW-R and conventional SG methods, using H_2O and ETG as solvent mixture, with different proportions ($0 < H_2O/ETG < 100\%$). XRD and Raman results confirmed that the obtained dominant crystal phase was Ant, in addition to traces of Brk or Rt phases that appeared in some samples. E_G calculations using K-M curves showed that they decreased by increasing Rt phase percentage. The high PC activity in E131 VF degradation occurred in 0% ETG SG and 0% ETG MW-R samples, due to higher surface area, and Rt phase absence. Kinetic evaluations showed that, as ETG percentage increased, NP PC performance decreased. This was due to the screen effect and blockage of the pores by ETG molecules, or by some combustion products that were produced during the samples calcination.

Acknowledgements

The author thanks the Lebanese University for providing financial assistance to carry out this work, and the American University of Beirut (AUB) for the help in doing the analysis in the KAS, CRSL laboratory.

Authors' contributions

F. Kassir: collected the data; did the preparation of the catalyst and the kinetic study and XRD and FTIR analysis (Master 2 student). **M. Azoury**: collected the data; did the preparation of the catalyst and the kinetic study and the Raman experiment (Master 2 student). **Z. Harajli**: collected the data; did the SEM and the UV reflection study DRS at AUB. **P. Damacet**: collected the data; did the BET and the DLS analysis at AUB. **M. El Jamal**: designed the analysis and selected the parameters for study; did the paper writing and editing. **Ebrahimian Pirbazari**: did the paper writing and editing.

Abbreviations

A: absorbance
Ant: anatase
AU: arbitrary unit
BET: Brunauer-Emmett-Teller
BP: boiling point
Brk: brookite
CVD: chemical vapor deposition
D: desorption
DLS: dynamic light scattering
DMSO: dimethyl sulfoxide
DRS: differential reflectance spectroscopy
E131 VF: food dye
EDX: energy dispersive X-ray spectrometer
E_G: bandgap energy
ETG: ethylene glycol
FTIR: Fourier-transform infrared spectroscopy

FWHM: full width at half maximum
KBr: potassium bromide
K-M: Kubelka-Munk
LOD: limit of detection
MW: microwave
MW-R: microwave-assisted reflux
NP: nanoparticles
NS: nanostructures
PC: photocatalytic
PI: polydispersity index
RC: rate constant
Rt: rutile
SEM: scanning electron microscopy
SG: sol-gel
TiO_2: titanium dioxide
TTIP: titanium IV isopropoxide
XRD: X-ray diffraction

Symbols definition
δ: loss tangent
μ: dipole moment
λ_{max}: maximum wavelength

References
1. Khan S and Ali J. Chemical analysis of air and water, Bioassays; 2018:21-39. http://dx.doi.org/10.1016/B978-0-12-811861-0.00002-4
2. Saidan MN, Al-Addous M, Al-Weshah RA et al. Wastewater Reclamation in Major Jordanian Industries: A Viable Component of a Circular Economy. Water. 2020;12:1276. http://doi.org/10.3390/w12051276
3. Velusamy S, Roy A, Sundaram S et al. A Review on heavy metal ions and containing dyes removal through graphene oxide-based adsorption strategies for textile wastewater treatment. Chem Rec. 2021,21:1570-1610. http://doi.org/10.1002/tcr.202000153
4. Gupta VK, Suhas. Application of low-cost adsorbents for dye removal-a review. J Environ Manag. 2009;(8)90;23:13-42. http://doi.org/10.1016/j.jenvman.2008.11.017
5. Dong H, Zeng G, Tang L et al. An overview on limitations of TiO2-based particles for photocatalytic degradation of organic pollutants and the corresponding countermeasures. Water Res. 2015;9:128-146. http://doi.org/10.1016/j.watres.2015.04.038
6. Saquib M, Abu Tariq M, Faisal M et al. Photocatalytic degradation of two selected dye derivatives in aqueous suspensions of titanium dioxide. Desalination. 2008;(219)1-3:301-11.
7. Chen C-C, Lu C-S, Mai F-D et al. Photooxidative N-de-ethylation of anionic triarylmethane dye (sulfan blue) in titanium dioxide dispersions under UV irradiation. J Haz Mater. 2006;137(3):1600-7.
8. Bessekhouad Y, Robert D, Weber JV. Preparation of TiO_2 nanoparticles by Sol-Gel route. Inter J Photoenergy. 2003;5:153-158. ID 496128. https://doi.org/10.1155/S1110662X03000278

9. Djaoued Y, Bruning R, Bersani D et al. Sol–gel nanocrystalline brookite-rich titania films. Mater Lett. 2004;58:2618-2622. http://doi.org/10.1016/S0167-577X(04)00227-7
10. Nam CT, Yang WD, Duc LM. Solvothermal synthesis of TiO_{10} photocatalysts in ketone solvents with low boiling points. J Nanomater. 2013;1-11. http://dx.doi.org/10.1155/2013/627385
11. Feng J, Zhang Z, Gao M et al. Effect of the solvents on the photocatalytic properties of $ZnFe_2O_4$ fabricated by solvothermal method. Mater Chem Phys. 2019,223:758-761.
12. Nguyen VN, Nguyen NKT, Nguyen PH. Hydrothermal synthesis of Fe-doped TiO_2 nanostructure photocatalyst. Adv Nat Sci: Nanosci Nanotechnol. 2011;2(3):035014.
13. Pradhan SK, Reucroft PJ, Yang F et al. Growth of TiO_2 nanorods by metalorganic chemical vapor deposition. J Cryst Growth, 2003;256:83-88.
14. Falk GS, Borlaf M, López-Muñoz MJ et al. Microwave-assisted synthesis of TiO_2 nanoparticles: photocatalytic activity of powders and thin films. J Nanopart Res. 2018;(20)23. https://doi.org/10.1007/s11051-018-4140-7
15. Vinodhini J, Mayandi J, Atchudan R et al. Effect of microwave power irradiation on TiO_2 nano-structures and binder free paste screen printed dye sensitized solar cells. Ceram Int. 2019;(4)45:4667-4673.
16. Jalawkhan RS, Ouda AA, Abdul-lettif AM et al. Effect of solvents on the morphology of TiO_2 nanoparticles prepared by microwave method. 2020. 2nd Int. Sci. Conference of Al-Ayen University (ISCAU-2020).
17. Bregadiollia BA, Fernandesa SL, Graeff CF de Oliveira. Easy and fast preparation of TiO_2 - based nanostructures using microwave assisted hydrothermal synthesis. Mater Res. 2017;20(4):912-919.
18. Pinjari DV, Prasad K, Gogate PR et al. Synthesis of titanium dioxide by ultrasound assisted sol–gel technique: Effect of calcination and sonication time. Ultrasonics Sonochem. 2015;23:185-191.
19. Sánchez-Hernández A K, Martínez-Juárez J, Gervacio-Arciniega JJ et al. Effect of ultrasound irradiation on the synthesis of hydroxyapatite/Titanium oxide nanocomposites. Crystals. 2020;10:959. http://doi.org/10.3390/cryst10110959
20. Shirsath SR, Pinjari DV, Gogate PR et al. Ultrasound assisted synthesis of doped TiO_2 nano-particles: Characterization and comparison of effectiveness for photocatalytic oxidation of dyestuff effluent. Ultrason Sonochem. 2012; (20)1:277-86. http://doi.org/10.1016/j.ultsonch.2012.05.015
21. Makki FA, El Haj Hassan MA, El Jamal MM et al. Kinetic evaluation of photocatalytic degradation of food colorant E 131 VF by copper doped TiO_2 nanophotocatalysts prepared at different calcination temperatures. Environ Technol Innovation. 2020;19;100981.
22. Gillespie PM. Microwave chemistry- An approach to the assessement of chemical reaction hazards. Symposium Series No. 1502004 IChemE.
23. Gawande MB, Shelke SN, Zboril R et al. Microwave-Assisted Chemistry: Synthetic applications for rapid assembly of nanomaterials and organics. Acc Chem Res. 2014;47:1338-1348. http://dx.doi.org/10.1021/ar400309b
24. Abubakar SM. Effect of Microwave Radiation on Organic Solvents. Experimen Findi. 2020. http://dx.doi.org/10.13140/RG.2.2.12381.36327

25. Akram M, Hussein R, Butt FK et al. Study of the effect of microwave holding time on the physicochemical properties of titanium oxide. Mater Res Express. 2019;6;8. https://doi.org/10.1088/2053-1591/ab1a0b
26. Ulises Z-L, Juan Z-M, Rafael R-T et al. Effect of temperature, pressure and power in obtaining TiO_2 and TiO_2-Fe via microwaves and evaluation of photocatalytic activity with synthesis time. Acta Univ. 2019;29:113. https://doi.org/10.15174/au.2018.1734
27. Barakat M, Khoder R, Kassir F et al. Sol-Gel to prepare Nickel doped TiO_2 nanoparticles for photocatalytic treatment of E 131 VF Food Dye Wastewater. J Water Environ Nanotechnol. 2021;37;(2)6:92-108.
28. El Tfayli M, Makki F, Kasir M et al. Photocatalytic Removal of Food Colorant E 131 VF from synthetic wastewater by Cu doped TiO_2 samples. J Water Environ Nanotechnol. 2019;4:87-197.
29. Jiang X, Wang Y, Herricks T et al. Ethylene glycol-mediated synthesis of metal oxide nanowires. J Mater Chem. 2004;14:695-703.
30. Stephane GC, El Jamal MM. Effect of doping of TiO_2 nanoparticles with silver on their photocatalytic activities toward degradation of E 131 VF. J Chem Technol Metall. 2019;54(5):926-933.
31. Khairuddin P, Utomo SB, Wulandari V et al. FTIR studies on the effect of concentration of polyethylene glycol on polimerization of Shellac. J Physics: Conference Series, Vol. 776, 8th Inter. Conference on Physics and its Applications (ICOPIA) 23-24 August 2016, Denpasar, Indonesia.
32. Quanjun L, Liu B, Ran YL et al. Ethylene glycol-mediated synthesis of nanoporous anatase TiO_2 rods and rutile TiO_2 self-assembly chrysanthemums. J Alloys Comp. 2009;(471)1-2:477-480.
33. Alyani SJ, Pirbazari AE, Khalilsaraei FE et al. Growing Co-doped TiO_2 nanosheets on reduced graphene oxide for efficient photocatalytic removal of tetracycline antibiotic from aqueous solution and modeling the process by artificial neural network. J Alloys Compd. 2019;799:169-182. http://dx.doi.org/10.1016/j.jallcom.2019.05.175
34. Choudhury B, Dey M, Choudhury A. Defect generation, d-d transition, and band gap reduction in Cu-doped TiO_2 nanoparticles. Int Nano Lett. 2013;(1)3;25.
35. Chalastara K, Guo F, Elouatik S et al. Tunable composition aqueous-synthesized mixed-phase TiO_2 nanocrystals for photo-Assisted Water Decontamination: Comparison of Anatase, Brookite and Rutile Photocatalysts. Catalysts. 2020;10(4):407.
36. Maddu A, Purwati R, and Kurniat M. Effects of poly-ethylene glycol (PEG) template on structural and optical properties of nanocrystalline titanium dioxide (TiO_2) films. J Ceram Process Res. 2016;(17)4:360-364.
37. Lagopati N, Tsilibry E-PH, Falaras P et al. Effect of nanostructured TiO_2 crystal phase on photoinduced apoptosis of breast cancer epithelial cells. Int J Nanaomed. 2014;(1)9:3219-3230. http://doi.org/10.2147/IJN.S62972.
38. Zhou C-H, Xu S, Yang Y. Titanium dioxide sols synthesized by hydrothermal methods using tetrabutyl titanate as starting material and the application in dye sensitized solar cells. Electrochim Acta. 2011;56:4308-4314.